International Journal of Nanomedicine

Dovepress
open access to scientific and medical research

Open Access Full Text Article

ORIGINAL RESEARCH

Biodegradable Eri silk nanoparticles as a delivery vehicle for bovine lactoferrin against MDA-MB-231 and MCF-7 breast cancer cells

This article was published in the following Dove Press journal:
International Journal of Nanomedicine
21 December 2015
Number of times this article has been viewed

Kislay Roy[1,*]
Yogesh S Patel[1,*]
Rupinder K Kanwar[1]
Rangam Rajkhowa[2]
Xungai Wang[2]
Jagat R Kanwar[1]

[1]Nanomedicine-Laboratory of Immunology and Molecular Biomedical Research (NLIMBR), Centre for Molecular and Medical Research (C-MMR), School of Medicine (SoM), Faculty of Health, [2]Institute for Frontier Materials (IFM), Deakin University, Waurn Ponds, VIC, Australia

*These authors contributed equally to this work

Abstract: This study used the Eri silk nanoparticles (NPs) for delivering apo-bovine lactoferrin (Apo-bLf) (~2% iron saturated) and Fe-bLf (100% iron saturated) in MDA-MB-231 and MCF-7 breast cancer cell lines. Apo-bLf and Fe-bLf-loaded Eri silk NPs with sizes between 200 and 300 nm (±10 nm) showed a significant internalization within 4 hours in MDA-MB-231 cells when compared to MCF-7 cells. The ex vivo loop assay with chitosan-coated Fe-bLf-loaded silk NPs was able to substantiate its future use in oral administration and showed the maximum absorption within 24 hours by ileum. Both Apo-bLf and Fe-bLf induced increase in expression of low-density lipoprotein receptor-related protein 1 and lactoferrin receptor in epidermal growth factor (EGFR)-positive MDA-MB-231 cells, while transferrin receptor (TfR) and TfR2 in MCF-7 cells facilitated the receptor-mediated endocytosis of NPs. Controlled and sustained release of both bLf from silk NPs was shown to induce more cancer-specific cytotoxicity in MDA-MB-231 and MCF-7 cells compared to normal MCF-10A cells. Due to higher degree of internalization, the extent of cytotoxicity and apoptosis was significantly higher in MDA-MB-231 (EGFR+) cells when compared to MCF-7 (EGFR–) cells. The expression of a prominent anti-cancer target, survivin, was found to be downregulated at both gene and protein levels. Taken together, all the observations suggest the potential use of Eri silk NPs as a delivery vehicle for an anti-cancer milk protein, and indicate bLf for the treatment of breast cancer.

Keywords: breast cancer, silk nanoparticles, bovine lactoferrin, epidermal growth factor receptor, apoptosis

Introduction

With 12.7 million new cancer cases and 7.6 million cancer deaths in 2008 worldwide, cancer has become the leading cause of death in developing countries and the second leading cause of death in developed countries.[1] Lung, prostate, breast, colorectal, and liver cancers are the most common types of cancers diagnosed every year. Breast cancer with 458,400 deaths, and colorectal cancer with 288,100 deaths in 2008 worldwide, became the leading types of cancer in females, whereas in males, the leading types of cancer were lung and bronchus cancer with 951,000 deaths, and liver cancer with 458,000 deaths in the same year. Breast, prostate, and colorectal cancer are the most common types of cancers found in Australia and New Zealand.[1]

Though cancer is the leading cause of death worldwide, it has limited treatment options, including chemotherapy, radiation therapy, laser therapy, and surgery. Among all the treatments available, chemotherapy is the most commonly used cancer treatment, but it has severe side effects, as most of the chemotherapeutic drugs directly affect cell division and DNA synthesis. Common side effects of using chemotherapeutic

Correspondence: Jagat R Kanwar
Nanomedicine-Laboratory of Immunology and Molecular Biomedical Research (NLIMBR), Centre for Molecular and Medical Research (C-MMR), School of Medicine (SoM), Faculty of Health, Deakin University, 75 Pigdons Road, Waurn Ponds, VIC 3217, Australia
Tel +61 3 5227 1148
Fax +61 3 5227 3402
Email jagat.kanwar@deakin.edu.au

drugs include anemia, leukemia, fatal infections, immune system depression, nausea, vomiting, hair loss, fatigue, and many more.[2]

The "red fraction", an undescribed protein from cow's milk later on known as lactoferrin, was first identified in 1939 by Sørensen and Sørensen.[3] The same lactoferrin from human and bovine milk was defined as transferrin-like glycol protein in 1960.[4] Initial studies revealed its biological role as anti-microbial, anti-viral, anti-fungal, anti-parasitic, anti-bacterial, and host defense immunomodulatory protein; also, its role in cell proliferation and differentiation was established.[5–8] The concept of oral administration of bovine lactoferrin (bLf) was first introduced during 1978 when a bLf-containing dry milk was marketed by Morinaga Milk company in Japan.[9] Later, the research and evidence indicated the role of orally administered bLf by reporting the improvement in intestinal microbial flora, increased serum ferritin and hematocrit levels, reduction in lower respiratory tract diseases, and anti-infective activities.[10–13]

Work done in our laboratory over the years has established bLf as an important anti-cancer natural therapeutic in different cancer models,[14–16] and we have also developed an efficient nanoparticle (NP) system for cancer-specific delivery of bLf. We have shown that natural bLf and iron-saturated forms of bLf (Fe-bLf) differ in their ability to augment cancer chemotherapy. By supplementing natural bLf (15% iron saturated), Apo-bLf (4% iron saturated), and 50% Fe-bLf into the diet of C57BL/6 mice that were subsequently challenged subcutaneously with tumor cells and were treated by chemotherapy, we found that Fe-bLf was a more potent natural adjuvant for augmenting cancer chemotherapy.[17] A previous study from our laboratory[18] has already established the anti-cancer activities of both Apo-bLf and Fe-bLf in MDA-MB-231 and MCF-7 cells. The results confirmed that the non-nanoformulated form of Apo-bLf induced significantly greater cytotoxicity and reduction in cell proliferation in both types of cancer cells. Most importantly it was also identified that key apoptotic molecules such as p53, Bcl-2, and survivin were significantly modulated by both forms of bLf.[18]

In another recent study,[19] we determined the anti-cancer efficacy and the internalization mechanism of our ceramic NP system (calcium phosphate nanocores, enclosed in biodegradable polymers, chitosan and alginate, alginate-enclosed chitosan-coated calcium phosphate nanocarriers (NCs) loaded with Fe-bLf in breast cancer xenograft model). We confirmed that Fe-bLf NCs decreased tumor size by 4.8-fold compared to void NCs and prevented tumor recurrence when compared to doxorubicin and Taxol® intra-peritoneal injections. The key receptors facilitating the NCs' internalization (low-density lipoprotein receptor related protein [LRP], lactoferrin receptor [LfR], and transferrin receptor [TfR]) were determined, and the micro-RNAs responsible for NC uptake were also identified.[19]

In the past 2 decades, the use of various types of NPs has yielded improved delivery of anti-cancer molecules to the tumor site. The most important benefit provided by the use of NPs is protection. Silk is mainly produced by cultured silkworms and several worms of the Lepidoptera family, including butterflies, and moths.[20] Silks are high-molecular weight co-polymer like proteins with extraordinary mechanical properties.[21,22] Crucial properties of silk, including biodegradability, biocompatibility, environmental stability, morphologic flexibility, controlled release, and small particle size. Silk can be used in combinational therapy as it can easily undergo chemical modifications, it is docile to organic or aqueous solvent processing, and the ability to modify amino acids in side chains to immobilize any biological compound, have broadened its uses in biomaterials and in a wide range of biomedical applications.[21,23] With extraordinary mechanical properties, naturally produced silk has gained much attention in past few years for its use in biomedical applications.[24–27] A study investigating the silk as a potential biomaterial for three-dimensional (3D) in vitro tumor modeling showed a better attachment and morphology of the MDA-MB-231 cell line on *Antheraea mylitta* silk matrices.[28] Eri silk is one such type of silk, which is very promising in producing a high quality silk powder with submicron particle size.[29] This promising strategy of producing Eri silk with submicron particle size has generated an interest of using this silk as a drug delivery vehicle to target cancer.

The primary objective of the present study was to compare the internalization of Eri silk (obtained from *Samia cynthia ricini* cocoons) NPs for delivering Apo-bLf and Fe-bLf, and the activation of downstream apoptosis mechanism involved in two different breast cancer cell lines.

Materials and methods

Silk NP preparation

Sodium carbonate, 2 g/L and sodium dodecyl sulphate, 0.6 g/L (Sigma-Aldrich Co, St Louis, MO, USA) at 100°C were used for degumming Eri silk cocoons. Chopping, attritor milling, bead milling, and spray drying were the techniques used to prepare the powder from degummed Eri silk cocoons. The degummed silk was chopped into snippets, which were further wet-milled using an attritor (S-1; Union

Process, Akron, OH, USA) containing 5 mm zirconium oxide milling media. Attritor speed was 280 rpm. To get nano silk particles, attritor-milled slurry was processed through a bead mill (Willy A Bachofen AG Maschinenfabrik, Basel, Switzerland). Zirconium oxide grinding media (0.4–0.5 mm) were used in bead milling. A milling speed of 1,500–3,500 rpm was used according to the manufacturer's recommendations. Cooling water (~18°C) was circulated through the milling chamber to minimize silk thermal degradation during milling. The milled slurry-in-water was used for further experiments.[29]

The prepared silk NPs, were washed three times with sterile phosphate-buffered saline (PBS) and were sonicated for 3 minutes to remove the aggregation prior to use. The pH of silk NP suspension was adjusted to 7.2 prior to use. Fe-bLf and Apo-bLf were loaded on the silk NPs with 10% w/w ratio, as determined by a previous study done in our laboratory.[30] The mixture (silk NPs + Fe-bLf or silk NPs + Apo-bLf) was incubated for 48 hours with slow stirring (30 rpm) at 4°C. After 48 hours, the samples were collected and centrifuged at 1,500 rpm for 20 minutes. The supernatant was collected and stored, and the pellet was washed two times using sterile PBS to remove unbound Fe-bLf or Apo-bLf. The sample was then lyophilized using a Labconco Freeze Dryer. A 1% solution of Fe-bLf-loaded silk NPs and Apo-bLf-loaded silk NPs was prepared from the lyophilized powder to calculate the loading efficiency. Protein estimation was performed to determine the amount of Fe-bLf or Apo-bLf loaded onto silk NPs. The amount of protein (Fe-bLf and Apo-bLf) loaded on silk NPs was also confirmed from the protein estimation of supernatant collected after 48 hours of stirring.

NP characterization

A 0.1% solution of prepared NPs was made by diluting 0.001 g of NPs in 1 mL of Milli-Q® water. The prepared 0.1% solution was further diluted to 10^4 by serial dilution. Finally, the obtained NP solution was mixed well, and the particle size was analyzed by dynamic light scattering (DLS) using Malvern Mastersizer. Lyophilized NPs were gently placed and distributed on a carbon tube, which was placed on an aluminum-based scanning electron microscopy (SEM) stub. The samples were then gold coated in a sputter coater (Quorum Technologies Ltd, Laughton, UK) for 60 seconds to avoid charging of the samples. SEM was performed for all the NPs using a Supra™ 55 variable pressure electron microscope. NP samples were crushed finely in an agate mortar and pestle, were mixed with potassium bromide (KBr), and were finely ground. Finally, the mixture was placed into a pelletizer to form the KBr disc containing the sample. The KBr disc was then analyzed using a Bruker Fourier transform infrared (FTIR) Vertex 70 spectrophotometer and Opus version 5.5 software (Bio-Rad Laboratories Inc, Hercules, CA, USA; Bruker Optics Inc, Billerica, MA, USA; Opus, Inc, Houston, TX, USA) in the wave number range of 400 to 4,000 cm^{-1}.

Rhodamine labeling of NPs

A 0.1% solution of Lissamine™ Rhodamine (Thermo Fisher Scientific, Waltham, MA, USA) was prepared to label a 1% solution of each NP. NPs and Rhodamine were mixed to make a total volume of 1 mL using Milli-Q in an Eppendorf tube® covered with aluminum foil. The tubes were placed on a rotor for 24 hours at 4°C for proper labeling of each NP. After 24 hours, the tubes were centrifuged, and the pellet was washed twice with PBS to remove the unbound Rhodamine; the pellet was then suspended in the treatment media prior to use. All steps related to Rhodamine labeling were performed in the dark to avoid loss of fluorescence.

Cell line and culture conditions

The MDA-MB-231 and MCF-7 adherent epithelial cell lines were derived from the mammary gland of breast adenocarcinomas in humans, and breast epithelial cells MCF-10A were obtained from the American Type Culture Collection (ATCC, Manassas, VA, USA). ATCC guidelines were followed in maintaining these cell lines.

Gel electrophoresis and Western blotting

Protein estimation results were used to calculate 80 µg (150 µg for cell lysate) of total protein per well. The samples were mixed with 10× sample buffer (with freshly added β-mercaptoethanol in a 1:10 ratio) and were allowed to heat at 95°C for 5 minutes. After loading the samples into each well, the gel (8%) was run at 200 V for 45 minutes using freshly prepared running buffer in a Mini PROTEAN® 3 gel tank (Bio-Rad Laboratories Inc). A protein standard marker (Bio-Rad Laboratories Inc) was used to compare the molecular weight of resulting bands from samples.

Using the Western blotting technique, proteins from a sodium dodecyl sulphate polyacrylamide gel electrophoresis (SDS-PAGE) gel were transferred onto polyvinylidene fluoride (Amersham™ Hybond™ enhanced chemiluminescence; GE health care and life sciences, Australia) membrane. After probing the membrane using specific antibodies, it was dried and activated in dark using 1 mL total enhanced chemiluminescence detection system solution (GE Healthcare

Bio-Sciences, Pittsburgh, PA, USA) for 2 minutes. The membrane was then viewed using Bio-Rad ChemiDoc with an XRS Camera. Images were captured and processed using Quantity One software.

Internalization studies

To determine the NP internalization, the MDA-MB-231 and MCF-7 cells were grown on eight-well slides in a 2×10^5 cells/mL concentration. When the cells were approximately 70%–75% confluent, they were treated with Rhodamine-labeled NPs for the time intervals of 4, 12, and 24 hours. After treatment, media were removed and the cell layer was washed thoroughly using sterile PBS. Slides were then fixed using 4% paraformaldehyde (PF) for 20 minutes at 37°C followed by 3× wash with PBS. The cell layer was blocked with 3% bovine serum albumin for 30 minutes and post-washing, was incubated with primary antibody (goat anti-bLf; Bethyl Laboratories, Inc, Montgomery, TX, USA) 1:100 for 1 hour. Post-washing, the cell layer was incubated with secondary fluorescein isothiocyanate (FITC)-conjugated antibody (anti-goat FITC; Sigma Aldrich Co) 1:100 for 1 hour. The cells were washed again, and mounting medium with 4′6-diamidino-2-phenylindole (DAPI), Vectashield® (Vector Laboratories, Burlingame, CA, USA) was added to each well, and the slides were covered using 22×50 mm cover slips. Nail polish was used to seal the ends of the slide to prevent over-drying. Slides were then viewed under a Leica TCS SP5 confocal microscope, and images were taken and processed using Leica software, LASAF.

Omnizyme® in vitro digestion

The Omnizyme (human digestive enzyme cocktail), commercially available proteolytic enzyme tablets, were purchased from Rainrock Nutritionals (Newark, OH, USA). Omnizyme and Omnizyme forte® are potent blends of vegetable and animal sources of proteolytic, amylytic, and lipolytic enzymes, which also contain the important free radical-fighters superoxide dismutase and catalase. These tablets also contain the enzyme activator glutathione, as well as lyophilized calf thymus and zinc. The Omnizyme tablet was dissolved in 15 mL of 0.1 M $NaHCo_3$ with a pH of 7.2. The samples (bLf-loaded NPs and plain bLf) and Omnizyme solution were mixed in the ratio of 1:50 and were incubated at 37°C at 200 rpm for the time intervals of 2, 4, 6, and 24 hours. The samples were collected after each incubation time and were heated at 42°C for 5 minutes to stop the reaction. All the samples were run on an SDS gel for further analysis of digestion.[31]

Intestinal loop assay

The intestinal loop assay was performed as per a previously published protocol.[32] Mice were sacrificed and intestines were removed by dissection. Duodenum, jejunum, and ileum sections were separated from each intestine and were incubated in sterile PBS. Each section of intestine was washed properly with PBS using a 23× G needle. One end of each section was tied using sterile thread, and Rhodamine-labeled NPs were injected from the open side. The open end was also tied after injecting the NPs, and the outer layer of the loop was washed in PBS. The loops were then incubated in six-well plates at 37°C with Roswell Park Memorial Institute (RPMI) 1640 culture medium without phenol red, 10% fetal bovine serum, and 1.5% penicillin streptomycin. Equal amounts of media were collected from each well after the time intervals of 6, 12, and 24 hours. The same amount of fresh medium was supplemented each time. After 24-hour incubation, the loop was opened and all sections were properly washed with sterile PBS. The sections were then fixed with 4% PF overnight, followed by freezing in optimum cutting temperature compound and storage at −80°C.[33,34]

Histopathology

Using cryotome, sections of 10 μm were cut and placed on a slide. The sections were than fixed in 100% acetone for 20 minutes. The slides were air dried and were stained with hematoxylin and eosin (HE). Slides were incubated in hematoxylin for 6 minutes, followed by washing twice with fresh water. Acid alcohol for 2–3 seconds was used to remove excessive hematoxylin staining from the tissue samples. Slides were again washed with fresh water, and then they were incubated in eosin for 1 minute. After cytoskeletal staining using eosin, slides were again washed twice with fresh water and were allowed to dry. The sections were dehydrated in gradients of ethanol, 70%, 90%, and 100%, for 2 minutes each. The slides were completely dried after dehydrating and were mounted using normal mounting medium; 22×50 mm cover slips were used to cover the slides, and nail polish was applied to prevent over-drying. The tissue samples were then viewed under a microscope, and images were captured using a Zeiss axioscope 5 (Carl Zeiss Meditec AG, Jena, Germany) and modified using Adobe Photoshop. The slides were also viewed using the confocal microscope by adding DAPI.

Cytotoxicity and apoptosis studies

A lactate dehydrogenase (LDH) assay was performed for cytotoxicity analysis as per the manufacturer's instructions (cytotoxicity detection kit; Hoffman-La Roche Ltd, Basel,

Switzerland). After 24-hour treatments with silk NPs only, silk NPs + Apo-bLf, silk NPs + Fe-bLf, Apo-bLf only, and Fe-bLf only at a concentration of 3,200 µg/mL, the supernatant was collected. The optical density (OD) was measured at 492 nm, and percentage cytotoxicity was calculated. Cells were also treated and stained with annexin V (apoptosis marker) and propidium iodide (PI) (necrosis marker) as per the manufacturer's instructions (annexin V assay; Thermo Fisher Scientific). The percentage population positive for annexin V or PI was determined using flow cytometry. Caspase-3 activity in the entire treatment group was measured using Acetyl-Asp-Glu-Val p-nitroanilide; Caspase-3 substrate was purchased from Sigma-Aldrich Co. The caspase activity was determined by following the directions given in the manufacturer's instructions. Absorbance was measured at 405 nm, and caspase-3 activity was calculated in mmol/mL concentration by using the following formula,

$$\text{Caspase-3 activity (mM/mL)} = \frac{\text{OD at 405 nm} \times \text{dilution factor (100)}}{[\text{E (mmol constant)} \times \text{time of incubation in minutes} \times \text{volume of sample}]} \quad (1)$$

where value of the mmol constant is 10.5, incubation time is 3 hours, and volume of the sample is the amount of sample added for loading 100 µg of the sample.

Tumor spheroid assay

Exactly 100 µL of 0.1% agarose solution was added in each well of 96-well plates. Once agar was solidified, 10^3 (MCF-7 and MDA-MB-231) cells/well were added to the plate and were incubated for 7 days at 37°C with 5% CO_2. After 7 days, cells had formed nearly uniform spheroids in all the wells; the spheroids were treated for 24 hours with silk NPs only, silk NPs + Apo-bLf, silk NPs + Fe-bLf, Apo-bLf only, and Fe-bLf only at a concentration of 3,200 µg/mL. The surface area of tumor spheroids was measured using ImageJ software (US National institute of health [NIH], Bethesda, MD, USA), where the circumference tool was used to calculate the surface area in pixels, and the surface area was plotted as a graph.[32]

Gene expression studies

TRIzol® reagent (Thermo Fisher Scientific), a ready-to-use reagent for total ribonucleic acid (RNA) isolation from cells, was used to isolate RNA from the viable cells after 12-hour treatments with silk NPs only, silk NPs + Apo-bLf, silk NPs + Fe-bLf, Apo-bLf only, and Fe-bLf only at a concentration of 3,200 µg/mL in a six-well plate. SuperScript® III First-Strand Synthesis System for reverse transcriptase polymerase chain reaction (RT-PCR) (Thermo Fisher Scientific) was used for complementary DNA (cDNA) synthesis from isolated RNA. All the components required were supplied with the SuperScript kit. Quantitative RT-PCR (qRT-PCR) iQ5 (Bio-Rad Laboratories Inc) was used for gene expression studies. An appropriate cycle was created in the software depending on the annealing temperature of individual primers.

Immunocytochemistry

The cells were cultured in eight-well slides with a concentration of 2×10^5 cells/mL (250 µL/well). The treatment with silk NPs + Apo-bLf, silk NPs + Fe-bLf, and silk NPs only for 24 hours was done with an initial cell confluence of 80%. Silk NPs only and untreated cells were used as a control to check the effect of loaded protein. After each step, cells were washed three times with PBS. The treatment was removed after 24 hours, and the cell layer was washed with PBS following the fixing of the cells using 4% PF for 25 minutes. The cells were then permeabilized using 0.1% Triton™ X-100 for 15 minutes by keeping the slide on ice. A 2% rabbit serum with 3% H_2O_2 (250 µL/well) was used as a blocking solution for 90 minutes. Goat primary antibody (1:100) against bLf (200 µL/well) was used to probe bLf for 2 hours, followed by incubation in the horseradish peroxidase-conjugated (1:100) secondary antibody (200 µL/well) for 1 hour. To visualize immunoreactivity, immunoperoxidase staining using 3,3 Diaminobenzidine (DAB) substrate (Sigma-Aldrich Co) (100 µL/well) for 12 minutes was carried out. The slides were washed thoroughly after DAB staining with tap water and were mounted with permanent mounting medium.

Statistical analysis

Significant differences between all treatment groups were determined by comparing individual treatments with untreated results using the Student's *t*-test and Microsoft Excel. Results are presented with ± standard error of the mean (SEM). *P*-values ≤ 0.05 were considered as significant, and values of $P \leq 0.01$ were considered to be highly significant.

Results

Physicochemical characterization of silk-loaded bLf NPs

Apo-bLf and Fe-bLf were prepared from native bLf using the dialysis method, and their purity was detected by SDS-PAGE and Western blotting (Figure 1A [parts a, b, respectively]). DLS spectroscopy was used to determine the hydrodynamic size distribution profile of the NPs. Void silk NPs showed sizes ranging from 150 to 250 nm, whereas silk NPs loaded with

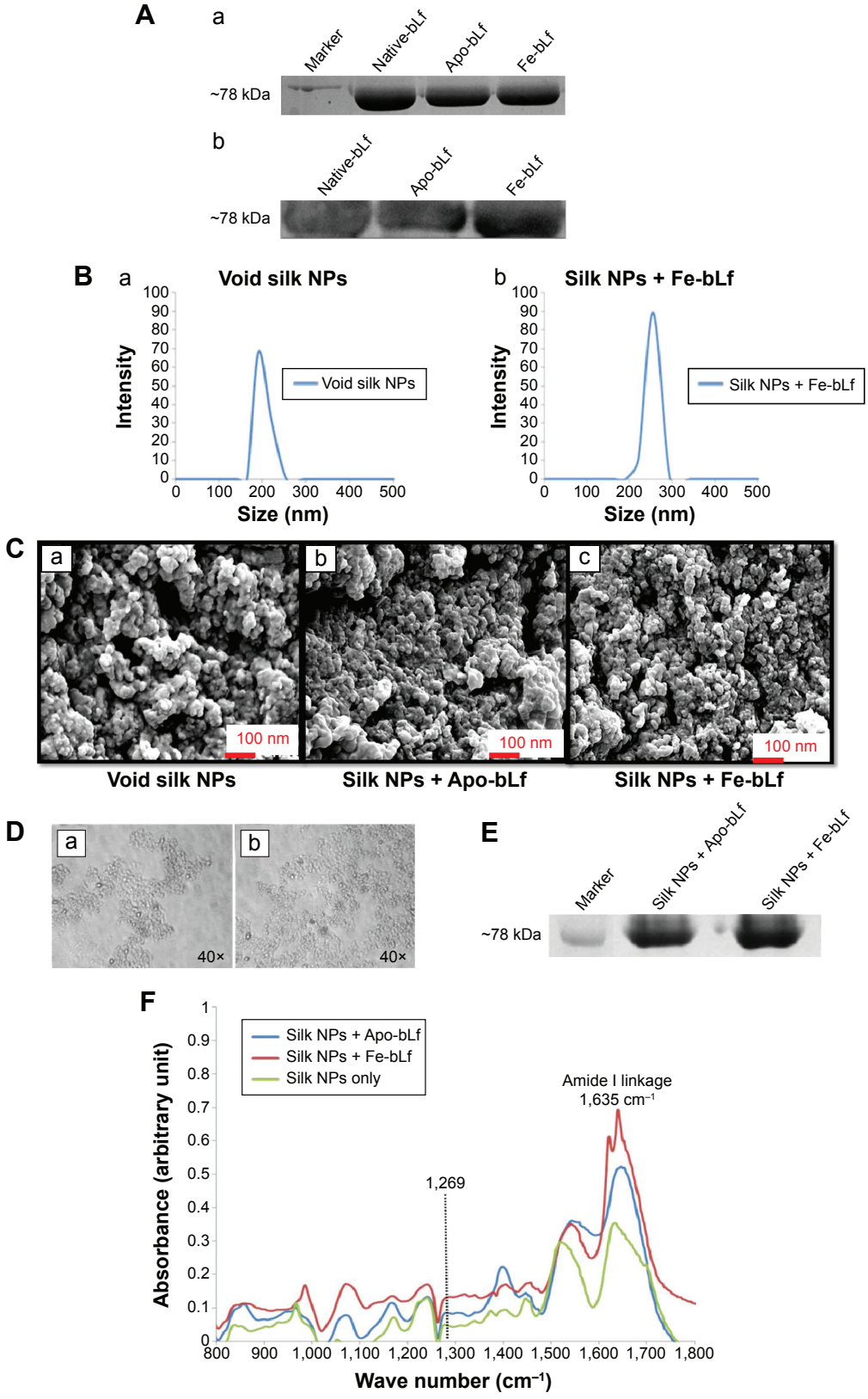

Figure 1 Characterization of silk + bLf NPs.

Notes: (**A**) Synthesis and purification of bLf forms was confirmed by (a) SDS-PAGE and (b) Western blotting. (**B**) DLS colorimetry confirmed the size of void NPs to be approximately 150–250 nm (a), while the silk + bLf NPs (b) were 200–300 nm in size. (**C**) SEM confirmed an irregular shape (a, b and c); however, NPs were of uniform size. (**D**) Sonication was used to prevent aggregation of (a) void, and (b) silk + bLf NPs, as seen in microscopic images obtained at 20× magnification. (**E**) Loading of bLf in silk NPs was confirmed using Western blotting. (**F**) FTIR spectra revealed the presence of amide peaks, confirming the loading of bLf on silk NPs.

Abbreviations: NP, nanoparticle; bLf, bovine lactoferrin; Apo-bLf, apo-bovine lactoferrin; Fe-bLf, iron-saturated bovine lactoferrin; SDS-PAGE, sodium dodecyl sulphate polyacrylamide gel electrophoresis; DLS, dynamic light scattering; SEM, scanning electron microscopy; FTIR, Fourier transform infrared.

Fe-BLf showed sizes ranging from 200 to 300 nm (Figure 1B [parts a, b, respectively]). SEM further confirmed the uniform size, morphology, shape, and pattern of the prepared NPs (Figure 1C). As Eri silk is known to aggregate[11] in solvents at pH >5, sonication for 3 minutes was used to disaggregate the silk particles in PBS at pH 7.2 just before loading the bLf. Figure 1D shows microscopic images of the nanomaterial at 40× magnification post-sonication, and these images depict loss of aggregation. Western blotting was performed to confirm the loading of bLf forms in silk NPs (Figure 1E). The peak at 1,269 cm^{-1} in the FTIR spectra represents the prominent α-helix structure.[9] Amide-I linkage at 1,635 cm^{-1} showed no change in the secondary structure in silk particles, whereas change in the intensity of peak was because of high binding affinity between silk particles and Apo-bLf and Fe-bLf (Figure 1F). Proteins tightly bound with silk particles could result in sustained release of protein, with a higher amount of protein released at the tumor site or in cancerous cells.

Receptor-mediated internalization of silk NPs in breast cancer cells

Confocal microscopy images reveal that void NPs failed to show substantial internalization in 4 hours in both MDA-MB-231 and MCF-7 cells, but managed to internalize at 24 hours (Figure 2A). Both silk + Apo-bLf and silk + Fe-bLf NPs showed significantly higher internalization at 4 and 24 hours in MDA-MB-231 cells, while only silk + Apo-bLf managed to show significant internalization in MCF-7 cells. In order to decipher the internalization patterns in these cells, qRT-PCR was performed to determine the expression of LRP1, LRP2, LfR, TfR, TfR1, and TfR2 in both MDA-MB-231 and MCF-7 cells (Figure 2B). It was found that MDA-MB-231 cells showed significantly higher expression of LRP1, LRP2, LfR, and TfR1 with silk NP treatments, while MCF-7 cells showed an increase in TfR and TfR2 receptor expression with treatments of silk NPs. This result confirmed that NPs internalized more in MDA-MB-231 cells due to the expression of more surface receptors.

Delivery of Apo-bLf and Fe-bLf in MDA-MB-231 cells

Void silk NPs were not able to internalize efficiently into cells after 12 hours. bLf-specific immuno-reactivity was observed as green (FITC) fluorescence in Figure 3A, which confirms the co-localization of Apo-bLf loaded on the silk NPs, as well as the presence of released protein in the cytoplasm and near the nucleus of the cells. Within 12 hours, Apo-bLf-loaded silk NPs were able to efficiently carry and release the loaded Apo-bLf into the cells. Yellow fluorescence (green + red) in the merged images of Figure 3A shows the detection of Apo-bLf loaded on silk NPs by the bLf-specific antibody. NPs were seen to be taken up by all MDA-MB-231 cells, with a maximum co-localization of NPs in the nucleus and cytoplasm of cells. Observations showing the fragmentation and distortion of cell layers and nuclei demonstrated the significantly high cytotoxic and anti-cancer effect of silk NPs loaded with Fe-bLf on MDA-MB-231 cells. Western blot analysis from protein lysates indicated the presence of bLf after 12 hours' treatment in MDA-MB-231 cells (Figure 3B). This result further proved the internalization of NPs in both MDA-MB-231 and MCF-7 cell lines, as studied using confocal microscopy. The images after the 24-hour treatment also revealed that NPs were internalized in MDA-MB-231 cells and induced cytotoxicity, while very low cytotoxicity could be observed in MCF-7 cells, as most NPs failed to internalize (Figure 3C).

Protection of bLf from enzymatic degradation and increased intestinal uptake

Digestion of bLf protein was confirmed using commercially available Omnizyme tablets. Unloaded Apo-bLf and Fe-bLf, and silk NPs loaded with Apo-bLf and Fe-bLf, were tested for digestion at different time intervals (Figure 4A [parts a, b]). That bLf forms loaded on silk NPs were digested by Omnizyme is probable, because it is not protected with any outer covering layer, and hence, it is directly available to the digestive enzyme. Compared to only protein, silk NP-loaded proteins were less digested, as bLf was strongly bound to NPs. Equal amounts of protein were loaded in each well to check the amount of digestion by Omnizyme. The maximum digestion of free and loaded bLf was observed after 24 hours of incubation with Omnizyme. After 6 hours, Rhodamine-labeled NPs were co-localized mainly in serosa, mucosal layers, and sub-mucosal layers of the ileum, as indicated by arrows (Figure 4B). NPs were also localized in the intestinal gland, crypt, and plicae circulares portion of the ileum. Hematoxylin and eosin staining confirmed the intact structure of ileum and mucoadhesion after 6 hours of incubation with Fe-bLf-loaded silk NPs (Figure 4C). The presence of bLf in various segments of intestinal tissue was confirmed by Western blotting, suggesting that silk NPs led to an enhanced uptake of bLf (Figure 4D).

bLf-loaded silk NP induced apoptosis in breast cancer cells

LDH assay results confirmed that bLf-loaded silk NPs led to specific cytotoxicity in MDA-MB-231 cells. Void silk

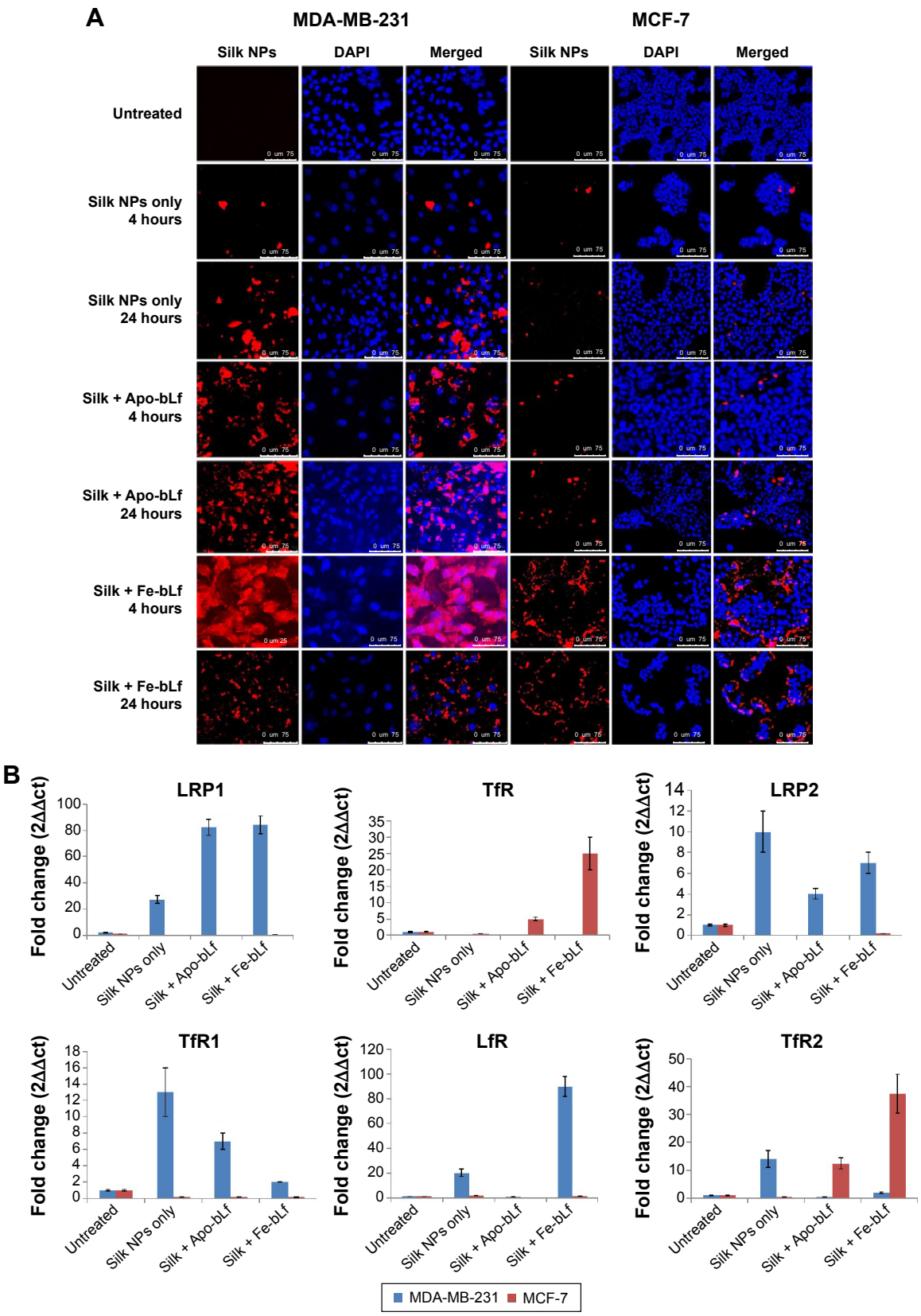

Figure 2 Internalization efficacy of silk + bLf NPs in breast cancer cells.

Notes: (A) Confocal images revealed that void NPs failed to significantly internalize in both MDA-MB-231 and MCF-7 cells. Silk + Apo-bLf showed comparatively higher internalization than silk + Fe-bLf in both MDA-MB-231 and MCF-7 cells. However, MDA-MB-231 cells showed significantly higher uptake of NPs than MCF-7 cells. (**B**) The gene expression of receptors revealed enhanced expression of LRP1, LRP2, LfR, and TfR1 in MDA-MB-231 cells, while only TfR1 and TfR2 were found to be upregulated in MCF-7 cells.

Abbreviations: DAPI, 4′6-diamidino-2-phenylindole; NPs, nanoparticles; bLf, bovine lactoferrin; Apo-bLf, apo-bovine lactoferrin; Fe-bLf, iron-saturated bovine lactoferrin; LRP, lipoprotein receptor-related protein; LfR, lactoferrin receptor; TfR, transferrin receptor.

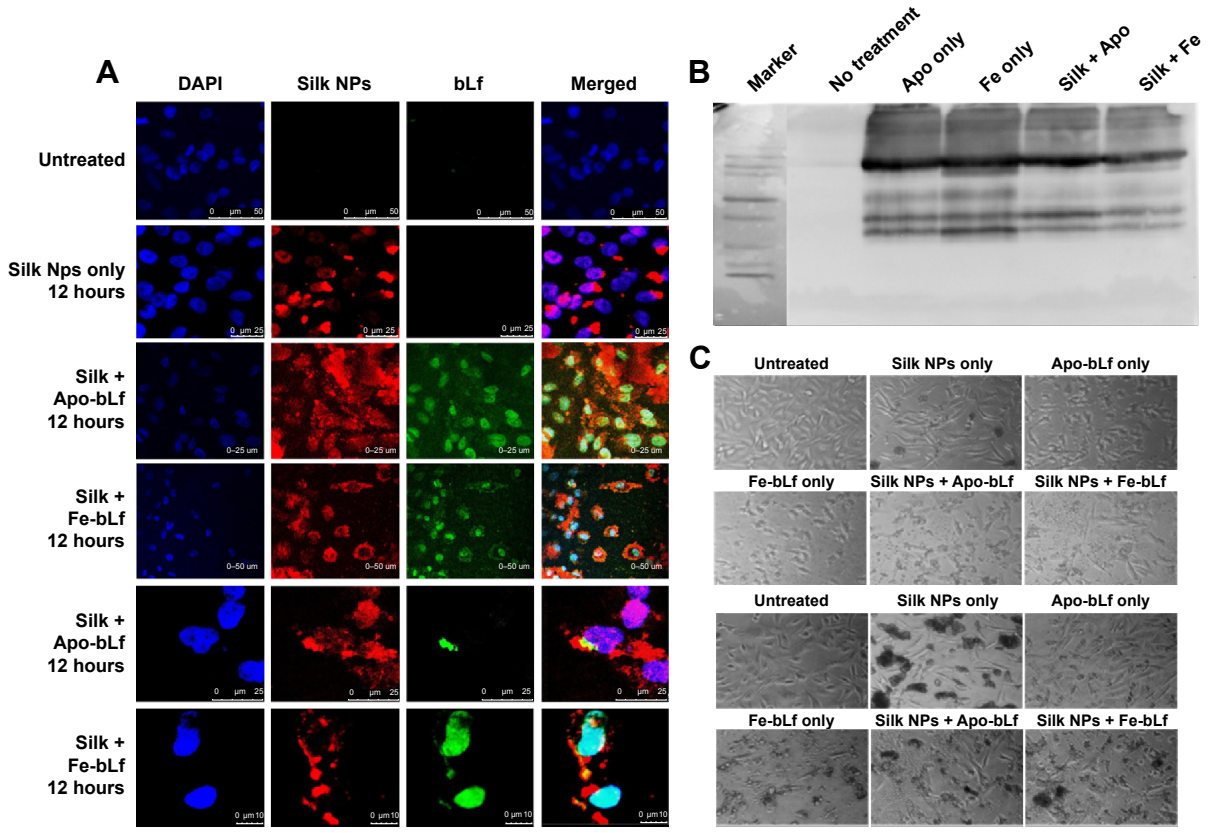

Figure 3 Silk NPs successfully delivered bLf into cells, inducing anti-cancer activity.
Notes: (**A**) The confocal microscopy images confirmed the presence of Apo-bLf and Fe-bLf (green) delivered by silk NPs (red) in the breast cancer cells (MDA-MB-231) within 12 hours. (**B**) Western blotting using the cell lysates also confirmed the presence of bLf forms in MDA-MB-231 cells. (**C**) The images from inverted microscopy revealed the presence of NPs in the media in MCF-7 cells, while most NPs were internalized by the MDA-MB-231 cells.
Abbreviations: DAPI, 4′6-diamidino-2-phenylindole; NPs, nanoparticles; bLf, bovine lactoferrin; Apo-bLf, apo-bovine lactoferrin; Fe-bLf, iron-saturated bovine lactoferrin; LRP, lipoprotein receptor-related protein; LfR, lactoferrin receptor; TfR, transferrin receptor.

NPs failed to induce significant cytotoxicity in primary (MCF-10A) as well as cancerous breast cells (MDA-MB-231, MCF-7) (Figure 5A). Nano-free forms of Apo-bLf and Fe-bLf showed significant cytotoxicity in both MDA-MB-231 and MCF-7 cells (88% and 72% apoptosis for Apo-bLf, respectively; and 79% and 78% apoptosis for Fe-bLf, respectively), while silk + Apo-bLf and silk + Fe-bLf forms induced significant cytotoxicity in only MDA-MB-231 cells (92% apoptosis for silk + Apo-bLf and 83% apoptosis for Fe-bLf). Annexin V assay was done to confirm apoptosis in treated breast cancer cells (Figure 5B). The results revealed that for MCF-7 cells, Apo-bLf led to only 36% apoptosis, while silk + Apo-bLf led to relatively higher apoptosis (47%), which was higher than for Fe-bLf only (26%) and Fe-bLf + silk (14%). For MDA-MB-231 cells, a similar trend was observed, where Apo-bLf only (50% apoptosis) and Apo-bLf + silk (52% apoptosis) led to higher apoptosis when compared to Fe-bLf only (28% apoptosis) and Fe-bLf + silk (33.5% apoptosis). Expression of caspase-3, which is the final activator of apoptosis, was detected by caspase-3 assay (Figure 5C). All treatments failed to induce any significant increase in caspase-3 expression in MCF-10A cells. It was observed that both Apo-bLf only and Fe-bLf only induced significantly higher caspase-3 expression in MDA-MB-231 cells (26% [$P<0.05$] and 28% [$P<0.05$], respectively) and in MCF-7 cells (17% and 24% [$P<0.05$], respectively). However, silk + Apo-bLf induced higher caspase-3 expression in MDA-MB-231 and MCF-7 cells (37.5% [$P<0.01$] and 30.1% [$P<0.05$], respectively) when compared to silk + Fe-bLf (25% [$P<0.05$] and 18%, respectively).

The results from multicellular tumor spheroid assay revealed that only silk NPs did not lead to any significant decrease in the size of tumor spheroids, while only Apo-bLf led to a 2-fold reduction in spheroid size ($P<0.01$) in both MCF-7 and MDA-MB-231 cells. Only Fe-bLf led to 1.7-fold reduction in tumor spheroid size in MDA-MB-231 cells ($P<0.01$), but only 1.23-fold reduction in MCF-7 cells. Silk NPs + Apo-bLf and silk NPs + Fe-bLf led to a significant reduction (1.8-fold [$P<0.0$] and 1.5-fold [$P<0.05$], respectively) in MDA-MB-231 cells (Figure 5D). However, both treatments failed to induce significant effects in MCF-7 cells.

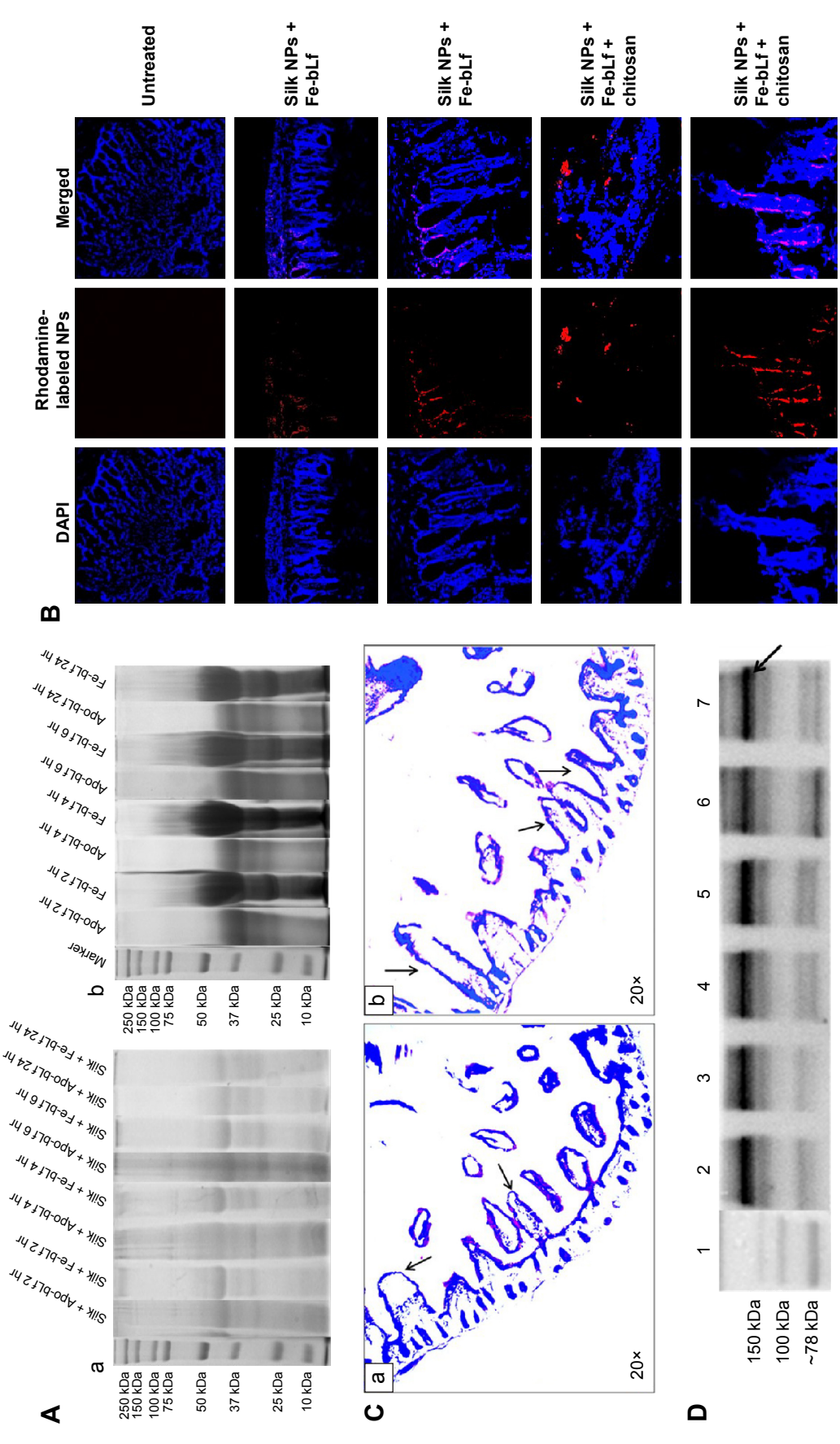

Figure 4 Omnizyme® and ex vivo loop assay.

Notes: (**A**) Omnizyme assay revealed comparatively higher stability of bLf in (b) silk + bLf forms when compared to (a) bLf alone. (**B**) Confocal images from the intestinal sections revealed the presence of Rhodamine-labeled silk NPs (red) in the intestinal sections. Magnification 40×. (**C**) Hematoxylin and eosin staining of structure and morphology of villi from ileum sections (40× magnification) incubated with (a and b) silk + bLf NPs. (**D**) Western blotting of Rhodamine-labeled silk + Fe-bLf collected from duplicate treatments of duodenum, jejunum, and ileum. Lane 1, the marker; lane 2, silk NPs + Fe-bLf duodenum 1; lane 3, silk NPs + Fe-bLf duodenum 2; lane 4, silk NPs + Fe-bLf jejunum 1; lane 5, silk NPs + Fe-bLf jejunum 2; lane 6, silk NPs + Fe-bLf ileum 1; and lane 7, silk NPs + Fe-bLf ileum 2.

Abbreviations: DAPI, 4′6-diamidino-2-phenylindole; NPs, nanoparticles; bLf, bovine lactoferrin; Apo-bLf, apo-bovine lactoferrin; Fe-bLf, iron-saturated bovine lactoferrin; hr, hours.

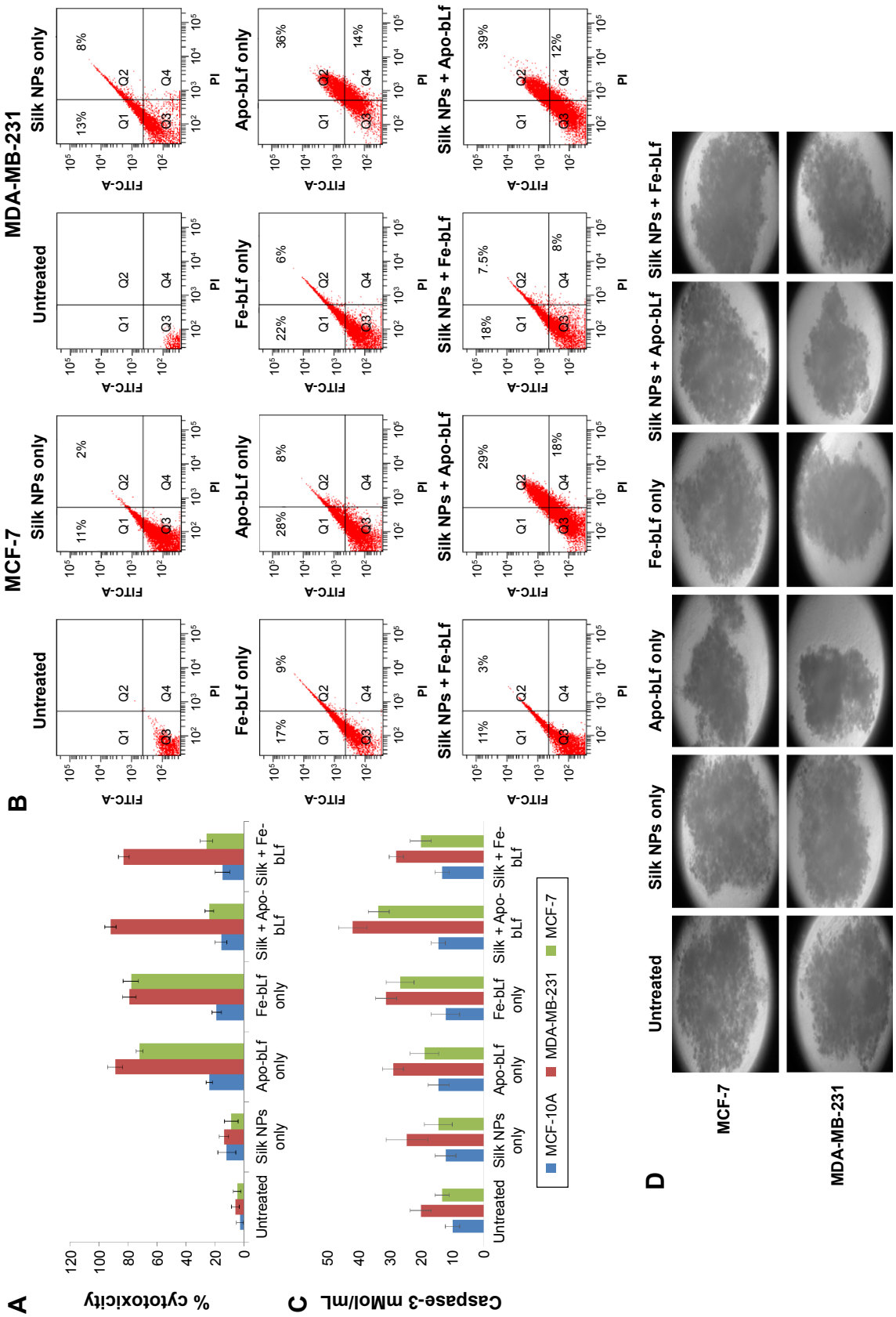

Figure 5 bLf forms specifically induce apoptosis in breast cancer cells.

Notes: (A) Percentage cytotoxicity determined using the LDH release revealed insignificant cytotoxicity in epithelial cells (MCF-10A), while higher cytotoxicity was found in cancer cells (MDA-MB-231 and MCF-7). (**B**) Annexin V assay results confirmed more apoptosis in MDA-MB-231 than in MCF-7 cells. Silk + Apo-bLf was found to be more effective than silk + Fe-bLf. (**C**) Caspase-3 release assay revealed that silk + Apo-bLf was found to be more effective than silk + Fe-bLf in inducing release of caspase-3. (**D**) Multicellular tumor spheroid assay results revealed that Apo-bLf and silk + Apo-bLf were more effective than Fe-bLf or silk + Fe-bLf in reducing tumor spheroid size.

Abbreviations: LDH, lactate dehydrogenase; NPs, nanoparticles; bLf, bovine lactoferrin; Apo-bLf, apo-bovine lactoferrin; Fe-bLf, iron-saturated bovine lactoferrin; FITC, fluorescein isothiocyanate; PI, propidium iodide; Q1, early apoptotic cells; Q2, both early and late apoptotic cells; Q3, live cells; Q4, late apoptotic cells.

Gene and protein expression for key apoptotic markers

qRT-PCR results (Figure 6A) revealed that bcl-2-like protein 4 (BAX), a pro-apoptotic effector protein of the Bcl-2 family responsible for permeabilizing the mitochondrial membrane during apoptosis, was observed to be upregulated in MDA-MB-231 cells (Figure S1). The significant upregulation of BAX was shown in MCF-7 cells after treatment with silk NPs loaded with Apo-bLf (Figure S2). In addition, the inner mitochondrial membrane protein, cytochrome C, was also upregulated in both MDA-MB-231 and MCF-7 cell lines. Caspase-9, an apoptotic gene of the caspase cascade, regulates via the intrinsic pathway; this gene was upregulated by 26-fold with non-formulated Apo-bLf treatment, and was 18-fold increased with nanoformulated Fe-bLf treatment of MDA-MB-231 cells. Caspase-9 was unaffected by silk + Fe-bLf, but was downregulated in all other treatments in MCF-7 cells, as shown in Figures 6A and S2. Caspase-8, an apoptotic gene of the caspase cascade regulated via extrinsic pathway, was upregulated in MCF-7 cells, whereas slight variation in gene expression of caspase-8 was observed in MDA-MB-231 cells. Caspase-3 and caspase-7, effector caspases from caspase family proteins, were upregulated in both MDA-MB-231 and MCF-7 cells with all the treatments, and significant upregulation was observed in silk NPs loaded with both forms of bLf. MDA-MB-231 and MCF-7 cells, when treated with 3,200 µg/mL of Apo-bLf and Fe-bLf alone, as well as after loading on silk NPs, showed downregulation of anti-apoptotic gene B-cell lymphoma-2 (Bcl-2) and survivin, and upregulation in apoptotic genes BAX, caspase-9, caspase-8, and caspase-3, which were involved in both apoptotic pathways. The death receptors, Fas and Fas-Ligand (Fas-L) of the extrinsic pathway, were upregulated in MCF-7 cells but were downregulated in MDA-MB-231 cells. Expression of tumor necrosis factor (TNF)-related apoptosis-inducing ligand (TRAIL) was also upregulated in both cell lines when treated with both the forms of bLf-loaded silk NPs. Immunoperoxidase staining results showed the maximum cytotoxic

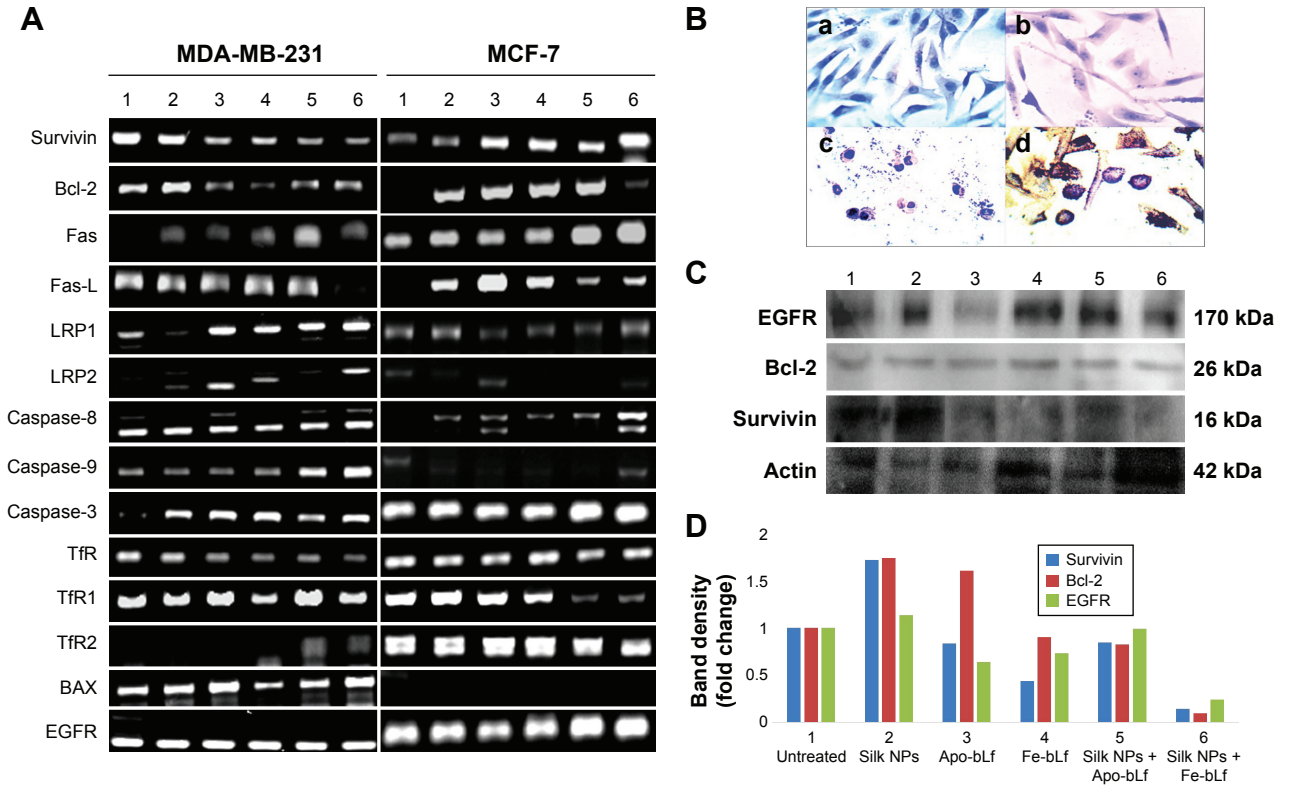

Figure 6 Gene and protein expression of key apoptotic markers.

Notes: (**A**) Genes were amplified using qRT-PCR iQ5, and graphs were plotted by calculating $2^{-\Delta\Delta C_t}$. (**B**) Immunocytochemistry for MDA-MB-231 cells treated with (a) untreated cells as a control, (b) silk NP only-treated cells, (c) silk NP + Fe-bLf-treated cells, and (d) silk NP + Apo-bLf-treated cells. (**C**) Western blotting assay to determine the effect of silk NPs + bLf on expression of EGFR, Bcl-2, and survivin. (**D**) Band density analysis for Western blots revealed that silk NPs + Fe-bLf was he most effective treatment. Lane 1, untreated; lane 2, silk NP only treated; lane 3, Apo-bLf only treated; lane 4, Fe-bLf only treated; lane 5, silk NPs + Apo-bLf treated; and lane 6, silk NPs + Fe-bLf treated.

Abbreviations: EGFR, epidermal growth factor receptor; Bcl, B-cell lymphoma-2; qRT-PCR, quantitative real-time polymerase chain reaction; NPs, nanoparticles; bLf, bovine lactoferrin; Apo-bLf, apo-bovine lactoferrin; Fe-bLf, iron-saturated bovine lactoferrin; LRP, lipoprotein receptor-related protein; LfR, lactoferrin receptor; TfR, transferrin receptor; BAX, Bcl-2-associated X protein; Fas, death receptor; Fas-L, Fas-ligand death receptor.

effect of silk NPs loaded with Fe-bLf after 24 hours in MDA-MB-231 cells (Figure 6B). Most of the cells were found dead, and the remaining cells were highly apoptotic, as confirmed by distorted nuclei and ruptured cytoplasm. On the other hand, 24 hours' treatment with silk NPs loaded with Apo-bLf was also observed to act against MDA-MB-231 cells, but the effect was less than from silk NPs loaded with Fe-bLf. A highly-colored brown reaction indicated the accumulation of Apo-bLf-loaded NPs in the cytoplasm and nuclei of the cells. This observation indicated that the protein was still available on the NPs and had not been utilized completely, hence indicating the efficiency of NPs to effectively protect and deliver Apo-bLf and Fe-bLf to MDA-MB-231 cells. Western blotting (Figure 6C) was performed to determine the expression of key apoptotic markers in MDA-MB-231 cells. Slight downregulation in EGFR was seen by Apo-bLf treatment (1.4-fold), whereas Fe-bLf and silk NPs + Apo-bLf did not show any downregulation in EGFR expression at protein level. Silk NPs + Fe-bLf were found to be the most effective in downregulating EGFR (5-fold downregulation). A significant downregulation in the expression of survivin was observed with Fe-bLf (2.5-fold) and silk NP + Fe-bLf (7-fold). Bcl-2 was also seen to downregulate with silk NP + Fe-bLf treatment (11-fold downregulation), but silk NP and Apo bLf treatments led to an increase in Bcl-2 expression (Figure 6D).

Discussion

Breast cancer, being one of the major and significant diseases in Western countries, affects one out of nine women in Australia.[35] To eradicate breast cancer completely, non-toxic, safe, non-invasive, and highly effective treatment is needed. Various anti-cancer peptides/proteins, including arginine-glycine aspartate peptide and antagonists to anti-apoptotic genes such as survivin antagonists, have been shown to boost anti-tumor effects and therapy. Quick renal clearance is one of the major hurdles faced while using these molecules in humans and rodents.[30,36] Considering its anti-cancer properties, natural availability, and its immune-modulation and immune-enhancing capacities, bLf is one of the ideal proteins that can be used to achieve maximum anti-cancer effects, without causing any toxicity to surrounding normal cells and tissues. Various studies on bLf, a natural milk protein, have proved its anti-cancer effects and lack of toxicity to normal cells.[15,30,37] In addition to its natural immune-modulation capacity,[17,40] bLf has also been shown to have immune-enhancing and anti-carcinogenic properties, because it can reduce chemically induced tumors in rats and humans.[17,37,41–42] The key findings of the current investigation suggest the efficient role of Eri silk NPs in carrying anti-cancer bLf proteins and inducing apoptosis using mitochondrial/intrinsic pathway of apoptosis.

Reports suggest that the internalization of bLf is facilitated by either TfR or LRP receptors.[18,30,35,42–44] Silk NPs alone were not able to internalize into the cells, even after 24 hours of incubation, whereas bLf-loaded silk NPs internalized within 2 hours. A previous study has shown that, generally, the silk polymer must be complexed with other polymers such as fibroin, and must be coated with ligands to increase internalization potential of NPs.[45] These findings generated our interest to look for the downstream mechanism and the receptors involved in the internalization of bLf-loaded silk NPs. qRT-PCR studies performed for the first time with Eri silk NPs loaded with bLf showed the significant upregulation of LRP1 in MDA-MB-231 cells, whereas no significant change in the expression of LRP1 was seen MCF-7 cells. TfRs including both TfR1 and TfR2 receptors did not show significant difference in treatments when compared to untreated and silk NP-treated MDA-MB-231 cells, suggesting the involvement of LRP1-, LRP2-, LfR-, and TfR1-mediated internalization of silk NPs loaded with bLf. In MCF-7 cells, TfR1 and TfR2 expression was significantly upregulated with silk NPs loaded with Fe-bLf treatment. Fas and Fas-L, responsible for the activation of the extrinsic pathway, were downregulated in MDA-MB-231 cells and upregulated in MCF-7 cells when treated with silk NPs loaded with both forms of bLf.

The results from the Omnizyme treatment confirmed that bLf forms in silk NPs showed comparatively higher resistance to Omnizyme when compared to non-nanoformulated bLf forms. A previous study from our laboratory has shown that bLf forms are prone to Omnizyme degradation; however, upon degradation, they give rise to a large C-lobe fragment (51 kDa), a small N-lobe fragment (36 kDa), and product fragments of non-homologous cleavage (~kDa).[46] Similar findings were observed in the present study, confirming that our findings are in accordance with the published reports.

The results of the ex vivo loop assay in the current study suggest the suitability of loaded bLf protein for absorption in various parts of the intestine, because of the presence of receptors in different parts of the intestine.[33,34] Western blot analysis illustrated that Fe-bLf loaded on silk NPs was present in the intact form after it was absorbed from the intestinal loops. This result showed the binding affinities of silk and bLf protein, as well as the ability of the Eri silk NPs to carry and successfully deliver the loaded bLf protein by maintaining

the intactness of bLf. The confocal microscopy images from 6-hour incubated ileum sections showed the absorption of silk NPs loaded with Fe-bLf by villi and co-localization in serosa, mucosal layers, and sub mucosal layers of the intestine.

Eri silk, being a biodegradable and biocompatible protein, showed no effect on MCF-10A, MDA-MB-231, and MCF-7 cells when administered alone. This result demonstrated the non-toxicity of Eri silk NPs to cells. Even though a previous publication from our lab suggested that Apo-bLf had higher cytotoxicity in both MDA-MB-231 and MCF-7 cells,[18] our current findings reveal that since silk NPs failed to significantly internalize in MCF-7 cells, cytotoxicity induced by both silk NPs + Apo-bLf or silk NPs + Fe-bLf in MCF-7 cells was lower than in MDA-MB-231 cells. It was also observed in our present study that Apo-bLf induced more apoptosis in both MCF-7 and MDA-MB-231 cells when compared to Fe-bLf.

Along with LRP1 receptors in MDA-MB-231 cells, EGFR and TRAIL expression were also upregulated with silk NPs loaded with bLf treatment. Similar upregulation in the expression of TRAIL was also observed in MCF-7 cells. EGFR is the most prominent transmembrane receptor that is responsible for the activation of series of intracellular pathways.[47] A study investigating DAB dendrimers in nanosystems showed that an upregulation in the expression of EGFR in human alveolar epithelial cell line A549 was responsible for uptake of dendrimers.[48] In the present study, we found that EGFR+ MDA-MB-231 cells showed higher expression of LRP and LfR receptors compared to EGFR– MCF-7 cells, which led higher uptake of silk + bLf NPs in MDA-MB-231 cells, and thus, more apoptosis and cytotoxicity in them when compared to MCF-7 cells (Figure 7).

The final outcome of any treatment is based on the capacity of the drug to induce apoptosis of the cancer cells. As bLf is known to activate the intrinsic pathway of apoptosis in oral carcinomas,[49] out current observations showing the downregulation of Bcl-2, an anti-apoptotic protein, the increase in cytochrome C (inner membrane protein), and

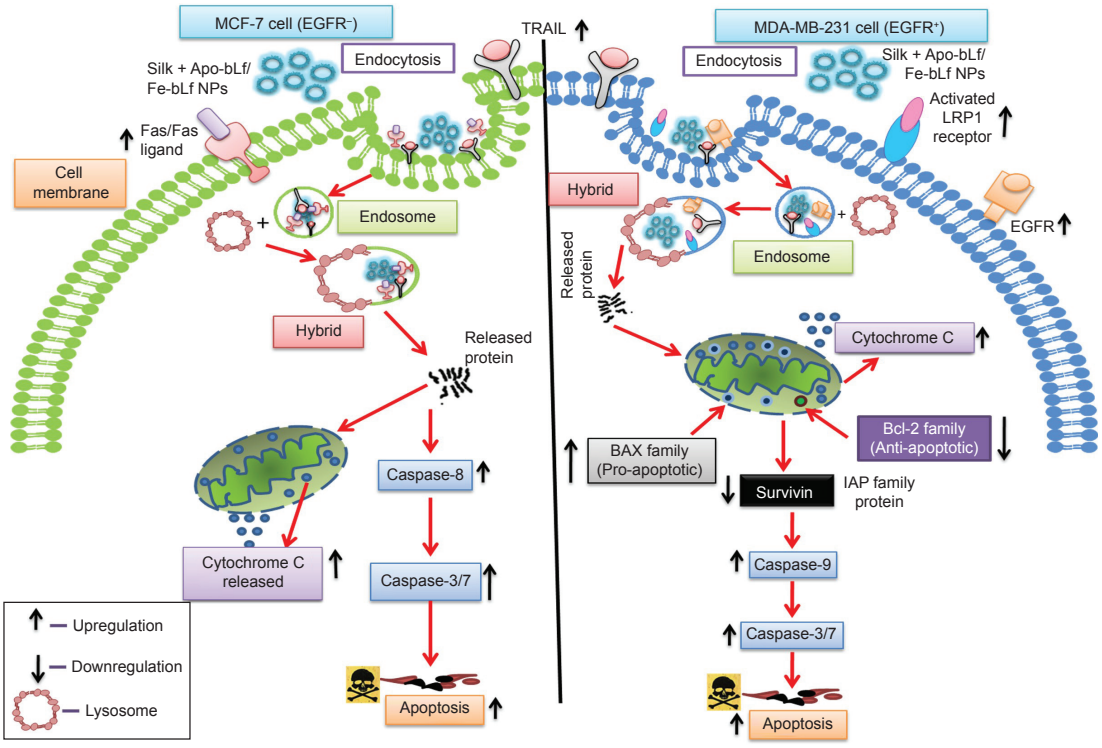

Figure 7 Silk + bLf NPs induced apoptosis in EGFR +ve and EGFR –ve cells.

Notes: Internalization of both forms of nanoformulation was facilitated via LRP1 receptors and EGFR in MDA-MB-231 cells and via death receptors in MCF-7 cells. In MDA-MB-231 cells, downregulation of anti-apoptotic genes and upregulation of apoptotic genes activated the intrinsic/mitochondrial pathway of apoptosis. In MCF-7 cells, apoptosis was mediated through upregulation of death receptors (Fas and Fas-L), caspase-8, and caspase-3 and -7, along with the upregulation in BAX. Black arrows in the figure show the upregulation and downregulation in gene expression. "Hybrid" denotes the formation of lyso-endosome (lysosome + endosome). Protein from NPs was released slowly inside the cells, and the unwanted materials, including NPs and receptors, were expunged by the cells via exocytosis. Red arrows are the signalling mechanism while black arrows are the effect of bLf on individual proteins/markers denoting upregulation or downregulation.

Abbreviations: IAPs, inhibitors of apoptosis proteins; EGFR, epidermal growth factor receptor; Bcl, B-cell lymphoma-2; NPs, nanoparticles; bLf, bovine lactoferrin; Apo-bLf, apo-bovine lactoferrin; Fe-bLf, iron-saturated bovine lactoferrin; LRP, lipoprotein receptor-related protein; LfR, lactoferrin receptor; TfR, transferrin receptor; BAX, Bcl-2-associated X protein; Fas, death receptor; TRAIL, tumor necrosis factor-related apoptosis-inducing ligand.

the upregulation of BAX, a pro-apoptotic protein, illustrate the activation of the intrinsic pathway of apoptosis in MDA-MB-231 cells when treated with silk NPs loaded with both forms of bLf. Apo-bLf, when used in non-nano-form, showed better anti-cancer effects compared to Fe-bLf in non-nano-form in MDA-MB-231 cells, but nanoformulated Fe-bLf showed better anti-cancer effects compared to any other form of treatment. In MCF-7 cells, no change in the genes involved in the intrinsic pathway was observed, except an increase in cytochrome C, which could be the result of loss of mitochondrial potential as cells go under apoptosis. The upregulation in caspase-8 in MCF-7 cells showed that apoptosis was mediated via activation of the extrinsic apoptotic pathway. Western blotting results were also in accordance with a previous study in which we found that both forms of bLf (Apo-bLf and Fe-bLf) led to downregulation of Bcl-2 and survivin.[18] Hence, our current findings confirm that bLf, when delivered using silk NPs, forms an efficient system to induce apoptosis in EGFR + ve breast cancer cells.

Conclusion

Successfully developed low particular size Eri silk NPs have a strong binding and loading ability for Apo-bLf and Fe-bLf. Silk NPs loaded with each of the forms of bLf were able to induce anti-cancer activity in both MDA-MB-231 and MCF-7 cell lines using different internalization and apoptosis mechanisms. The internalization studies and qRT-PCR results indicated, for first time, that Eri silk NPs loaded with Fe-bLf protein may be used for the treatment of breast cancers with EGFR, LRP, and TfR receptor expression. Fe-bLf, when used in nanoformulation, activated the intrinsic pathway of apoptosis by significant downregulation of anti-apoptotic molecules including survivin and Bcl-2, and by upregulation of pro-apoptotic and apoptotic genes such as BAX and caspases in MDA-MB-231 cells. The same nanoformulations were observed activating the extrinsic pathway and intrinsic pathway of apoptosis in MCF-7 cells. The maximum absorption of silk + Fe-bLf in the ileum and the intact structure of gut and villi suggest the use of Eri silk NPs in near future for further in vivo studies. Also, the ex vivo loop assay further suggests the use of chitosan-coated Eri silk NPs for oral administration. The outcome from the present study clearly indicates the role of bLf as a strong and promising therapeutic agent for breast cancer.

Acknowledgments

The authors would like to thank the Australia–India Strategic Research Fund (grant AISRF BF030016) and the National Health and Medical Research Council (grant NHMRC APP1050286) for financial support. Support from the Australian Research Council (ARC), through an ARC Discovery Grant (number DP120100139), is also acknowledged.

Disclosure

The authors have no other relevant affiliations or financial involvement with any organization or entity with a financial interest in or financial conflict with the subject matter or materials discussed in the manuscript. No writing assistance was utilized in the production of this manuscript.

References

1. Jemal A, Bray F, Center MM, Ferlay J, Ward E, Forman D. Global cancer statistics. *CA Cancer J Clin*. 2011;61(2):69–90.
2. Mita K, Kasahara M, Sasaki S, et al. The genome sequence of silkworm, *Bombyx mori*. *DNA Res*. 2004;11(1):27–35.
3. Sørensen M, Sørensen SPL. The proteins in whey. CR TraV Lab, Carlsberg, Copenhagen. 1939;23:55–99.
4. Johansson B. Isolation of crystalline lactoferrin from human milk. *Acta Chem Scand*. 1968;23(2):683–684.
5. Prasad MD, Muthulakshmi M, Arunkumar KP, et al. SilkSatDb: a microsatellite database of the silkworm, *Bombyx mori*. *Nucleic Acids Res*. 2005;33(Database issue):D403–D406.
6. Papanicolaou A, Gebauer-Jung S, Blaxter ML, Owen McMillan W, Jiggins CD. ButterflyBase: a platform for lepidopteran genomics. *Nucleic Acids Res*. 2008;36(Database issue):D582–D587.
7. Negre V, Hôtelier T, Volkoff A, et al. SPODOBASE: an EST database for the lepidopteran crop pest Spodoptera. *BMC Bioinformatics*. 2006;7:322.
8. Grimaldi D, Engel M. *Evolution of the Insects*. Cambridge: Cambridge University Press; 2005.
9. Dunning AM, Healey CS, Pharoah PDP, Teare MD, Ponder BAJ, Easton DF. A systematic review of genetic polymorphisms and breast cancer risk. *Cancer Epidemiol Biomarkers Prev*. 1999;8(10):843–854.
10. Croce CM. Oncogenes and cancer. *N Engl J Med*. 2008;358(5):502–511.
11. Knudson AG. Two genetic hits (more or less) to cancer. *Nat Rev Cancer*. 2001;1(2):157–162.
12. Zhang YQ. Applications of natural silk protein sericin in biomaterials. *Biotechnol Adv*. 2002;20(2):91–100.
13. Sasaki M, Kato N, Watanabe H, Yamada H. Silk protein, sericin, suppresses colon carcinogenesis induced by 1,2-dimethylhydrazine in mice. *Oncol Rep*. 2000;7(5):1049–1052.
14. Kanwar JR, Kanwar RK, Sun X, et al. Molecular and biotechnological advances in milk proteins in relation to human health. *Curr Protein Pept Sci*. 2009;10(4):308–338.
15. Gibbons JA, Kanwar RK, Kanwar JR. Lactoferrin and cancer in different cancer models. *Front Biosci (Schol Ed)*. 2010;3:1080–1088.
16. Kanwar RK, Kanwar JR. Immunomodulatory lactoferrin in the regulation of apoptosis modulatory proteins in cancer. *Protein Pept Lett*. 2013;20(4):450–458.
17. Kanwar JR, Palmano KP, Sun X, et al. 'Iron-saturated' lactoferrin is a potent natural adjuvant for augmenting cancer chemotherapy. *Immunol Cell Biol*. 2008;86(3):277–288.
18. Gibbons JA, Kanwar JR, Kanwar RK. Iron-free and iron-saturated bovine lactoferrin inhibit survivin expression and differentially modulate apoptosis in breast cancer. *BMC Cancer*. 2015;15:425.
19. Mahidhara G, Kanwar RK, Roy K, Kanwar JR. Oral administration of iron-saturated bovine lactoferrin-loaded ceramic nanocapsules for breast cancer therapy and influence on iron and calcium metabolism. *Int J Nanomedicine*. 2015;10:4081–4098.

20. Xia Y, Lu Y. Fabrication and properties of conductive conjugated polymers/silk fibroin composite fibers. *Compos Sci Technol*. 2008;68(6):1471–1479.
21. Vepari C, Kaplan DL. Silk as a biomaterial. *Prog Polym Sci*. 2007;32(8–9):991–1007.
22. Bini E, Knight DP, Kaplan DL. Mapping domain structures in silks from insects and spiders related to protein assembly. *J Mol Biol*. 2004;335(1):27–40.
23. Altman GH, Diaz F, Jakuba C, et al. Silk-based biomaterials. *Biomaterials*. 2003;24(3):401–416.
24. Wang X, Hu X, Daley A, Rabotyagova O, Cebe P, Kaplan DL. Nanolayer biomaterial coatings of silk fibroin for controlled release. *J Control Release*. 2007;121(3):190–199.
25. Lammel AS, Hu X, Park SH, Kaplan DL, Scheibel TR. Controlling silk fibroin particle features for drug delivery. *Biomaterials*. 2010;31(16):4583–4591.
26. Wang X, Yucel T, Lu Q, Hu X, Kaplan DL. Silk nanospheres and microspheres from silk/pva blend films for drug delivery. *Biomaterials*. 2010;31(6):1025–1035.
27. Wang X, Wenk E, Hu X, et al. Silk coatings on PLGA and alginate microspheres for protein delivery. *Biomaterials*. 2007;28(28):4161–4169.
28. Talukdar S, Mandal M, Hutmacher DW, Russell PJ, Soekmadji C, Kundu SC. Engineered silk fibroin protein 3D matrices for in vitro tumor model. *Biomaterials*. 2011;32(8):2149–2159.
29. Rajkhowa R, Wang L, Kanwar J, Wang X. Fabrication of ultrafine powder from eri silk through attritor and jet milling. *Powder Technol*. 2009;191(1–2):155–163.
30. Kanwar JR, Kanwar RK. Gut health immunomodulatory and anti-inflammatory functions of gut enzyme digested high protein micronutrient dietary supplement-Enprocal. *BMC Immunol*. 2009;10:7.
31. Roy K, Kanwar RK, Krishnakumar S, Cheung CH, Kanwar JR. Competitive inhibition of survivin using a cell-permeable recombinant protein induces cancer-specific apoptosis in colon cancer model. *Int J Nanomedicine*. 2015;10:1019–1043.
32. Kanwar RK, Ganguly NK, Kanwar JR, Kumar L, Walia BN. Impairment of Na+, K+-ATPase activity following enterotoxigenic *Campylobacter jejuni* infection: changes in Na+, Cl− and 3-O-methyl-D-glucose transport in vitro, in rat ileum. *FEMS Microbiol Lett*. 1994;124(3):381–385.
33. Kanwar RK, Ganguly NK, Kumar L, Rakesh J, Panigrahi D, Walia BN. Calcium and protein kinase C play an important role in *Campylobacter jejuni*-induced changes in Na+ and Cl− transport in rat ileum in vitro. *Biochim Biophys Acta*. 1995;1270(2–3):179–192.
34. Australian Institute of Health and Welfare (AIHW). Breast cancer in Australia: an overview, 2009. In: *Cancer Series Canberra*: *Australian Institute of Health and Welfare and National Breast and Ovarian Cancer Centre*. Bruce, ACT: AIHW. 2009:170.
35. Kanwar JR, Mahidhara G, Kanwar RK. Antiangiogenic therapy using nanotechnological-based delivery system. *Drug Discov Today*. 2011;16(5–6):188–202.
36. Ryan BM, O'Donovan N, Duffy MJ. Survivin: a new target for anti-cancer therapy. *Cancer Treat Rev*. 2009;35(7):553–562.
37. Kanwar JR, Mahidhara G, Kanwar RK. Novel alginate-enclosed chitosan-calcium phosphate-loaded iron-saturated bovine lactoferrin nanocarriers for oral delivery in colon cancer therapy. *Nanomedicine (Lond)*. 2012;7(10):1521–1550.
38. Damiens E, Mazurier J, el Yazidi I, et al. Effects of human lactoferrin on NK cell cytotoxicity against haematopoietic and epithelial tumour cells. *Biochim Biophys Acta*. 1998;1402(3):277–287.
39. Duarte DC, Nicolau A, Teixeira JA, Rodrigues LR. The effect of bovine milk lactoferrin on human breast cancer cell lines. *J Dairy Sci*. 2011;94(1):66–76.
40. Actor JK, Hwang SA, Kruzel ML. Lactoferrin as a natural immune modulator. *Curr Pharm Des*. 2009;15(17):1956–1973.
41. Iigo M, Kuhara T, Ushida Y, Sekine K, Moore MA, Tsuda H. Inhibitory effects of bovine lactoferrin on colon carcinoma 26 lung metastasis in mice. *Clin Exp Metastasis*. 1999;17(1):35–40.
42. Kanwar JR, Mahidhara G, Roy K, et al. Fe-bLf nanoformulation targets survivin to kill colon cancer stem cells and maintains absorption of iron, calcium and zinc. *Nanomedicine (Lond)*. 2015;10(1):35–55.
43. Ashida K, Sasaki H, Suzuki YA, Lönnerdal B. Cellular internalization of lactoferrin in intestinal epithelial cells. *BioMetals*. 2004;17(3):311–315.
44. Jiang R, Lopez V, Kelleher SL, Lönnerdal B. Apo- and holo-lactoferrin are both internalized by lactoferrin receptor via clathrin-mediated endocytosis but differentially affect ERK-signaling and cell proliferation in caco-2 cells. *J Cell Physiol*. 2011;226(11):3022–3031.
45. Subia B, Chandra S, Talukdar S, Kundu SC. Folate conjugated silk fibroin nanocarriers for targeted drug delivery. *Integr Biol (Camb)*. 2014;6(2):203–214.
46. Ebrahim F, Shankaranarayanan JS, Kanwar JR, Gurudevan S, Krishnan UM, Kanwar RK. Identification of unprecedented anticancer properties of high molecular weight biomacromolecular complex containing bovine lactoferrin (HMW-bLf). *PLoS One*. 2014;9(9):e106568.
47. Ciardiello F, Tortora G. EGFR antagonists in cancer treatment. *N Engl J Med*. 2008;358(11):1160–1174.
48. Omidi Y, Barar J. Induction of human alveolar epithelial cell growth factor receptors by dendrimeric nanostructures. *Int J Toxicol*. 2009;28(2):113–122.
49. Mohan KV, Gunasekaran P, Varalakshmi E, Hara Y, Nagini S. In vitro evaluation of the anticancer effect of lactoferrin and tea polyphenol combination on oral carcinoma cells. *Cell Biol Int*. 2007;31(6):599–608.

Supplementary materials

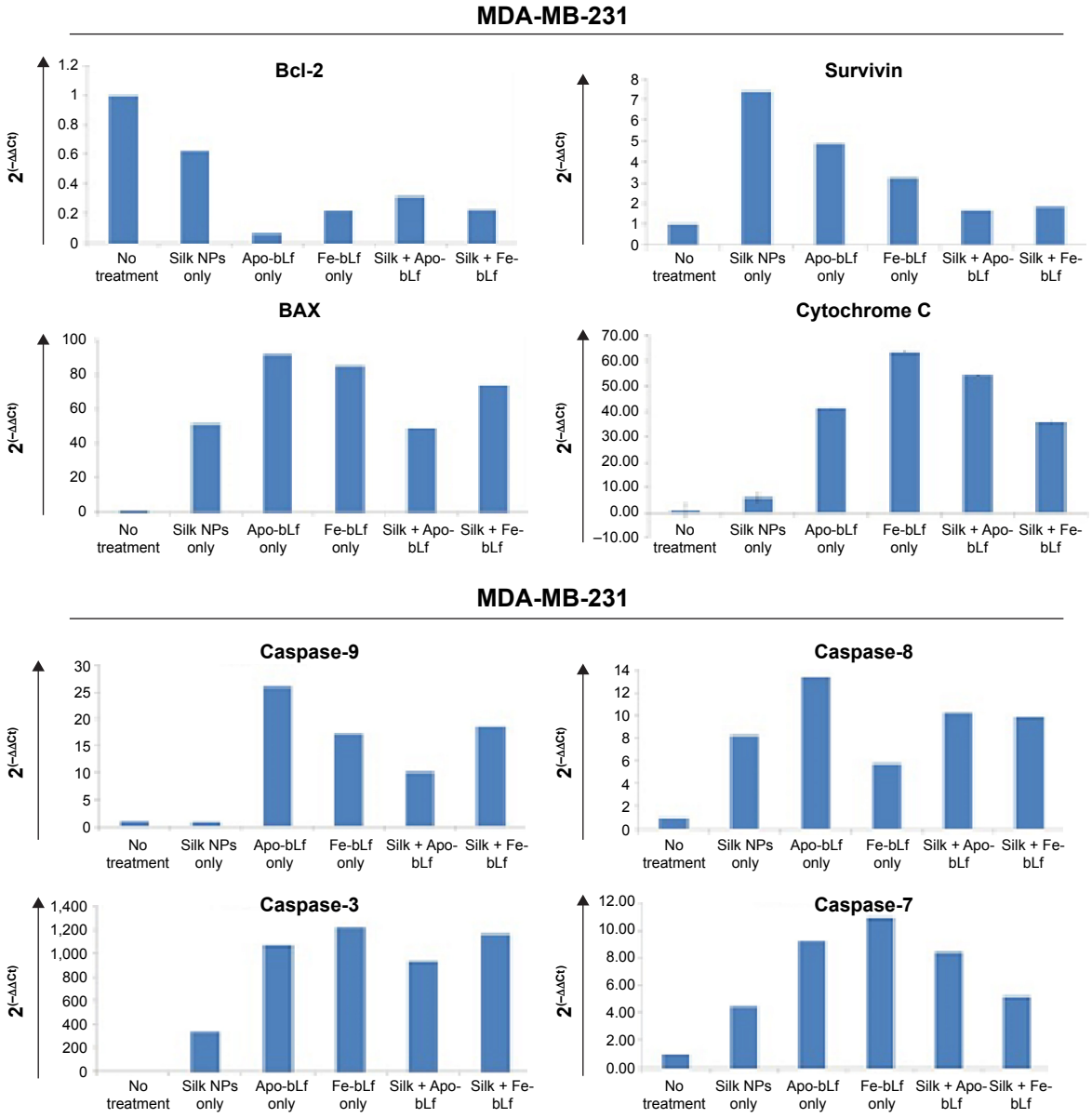

Figure S1 (*Continued*)

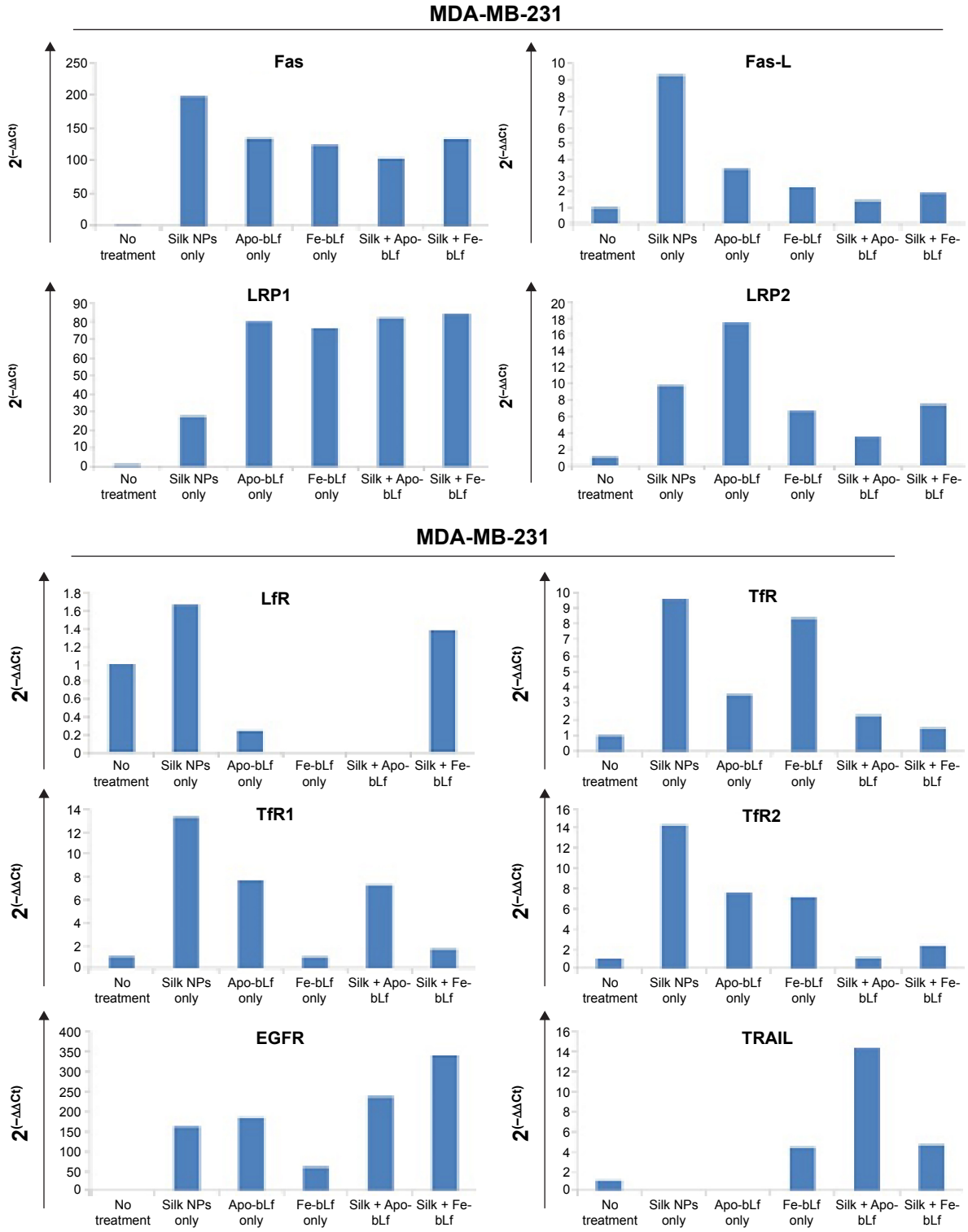

Figure S1 Fold change in gene expressions for MDA-MB-231 cells.
Note: Representative analysis for quantitative PCR analysis of key apoptotic markers and lactoferrin receptors.

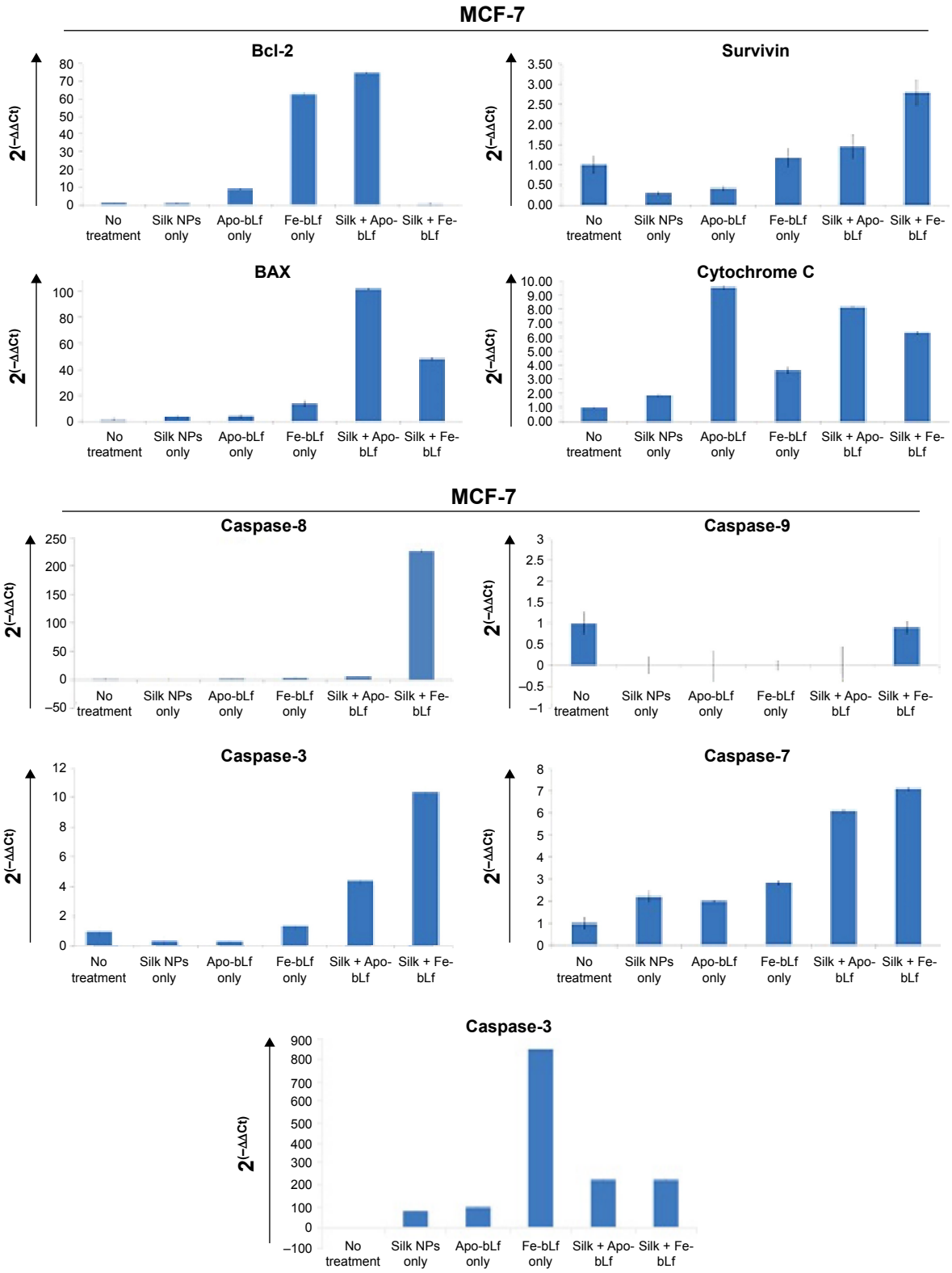

Figure S2 (*Continued*)

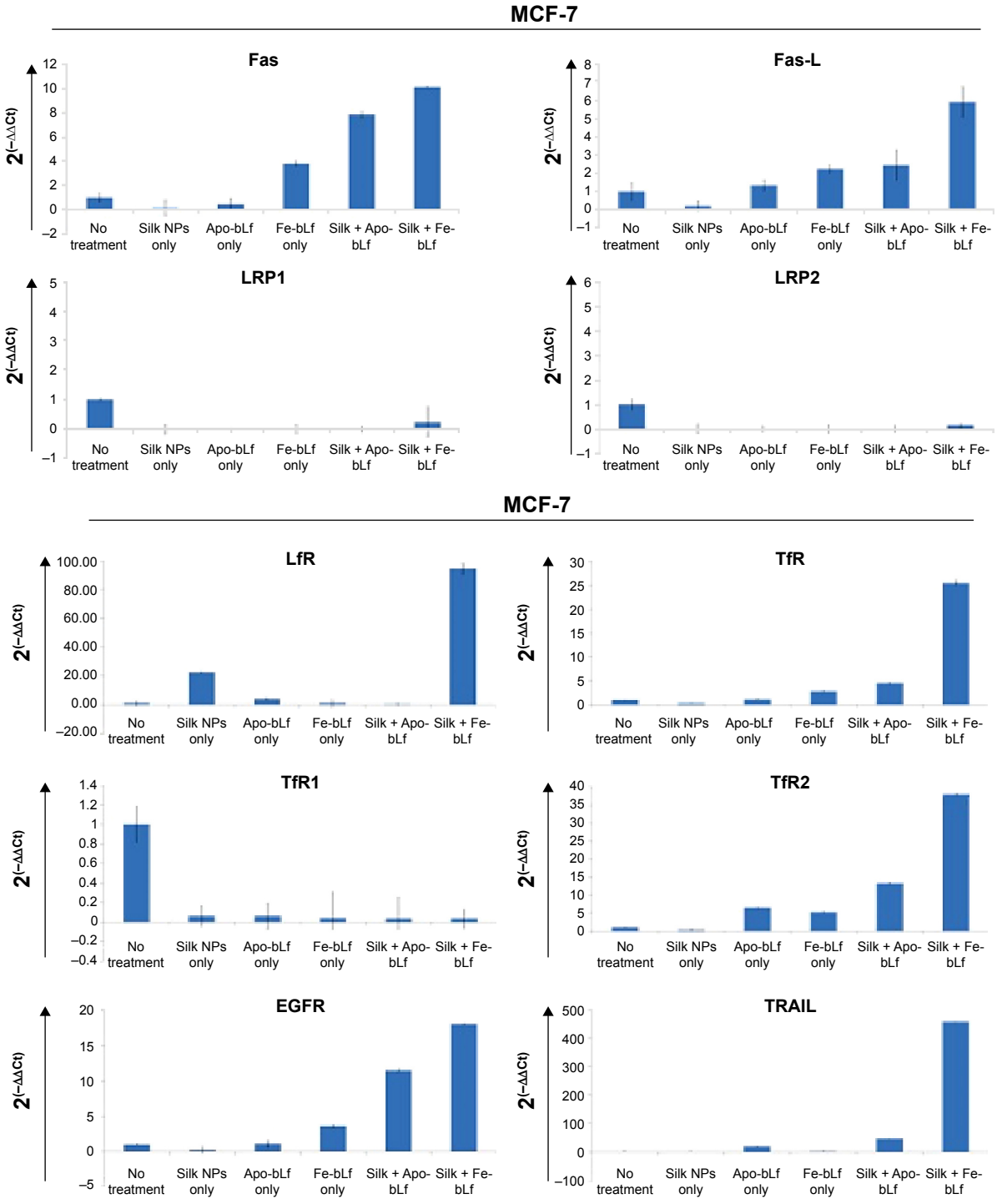

Figure S2 Fold change in gene expressions for MCF-7 cells.
Note: Representative analysis for quantitative PCR analysis of key apoptotic markers and lactoferrin receptors.